

# The structure of small lead clusters

Jonathan P. K. Doye\*

*University Chemical Laboratory, Lensfield Road, Cambridge CB2 1EW, United Kingdom*

Shaun C. Hendy

*Applied Mathematics, Industrial Research Limited, Lower Hutt, New Zealand*

(Dated: November 6, 2018)

We have located the global minimum for all lead clusters with up to 160 atoms using a glue potential to model the interatomic interactions. The lowest-energy structures are not face-centred cubic as suggested previously. Rather, for  $N < 40$  the majority of structures are decahedral or hexagonal close-packed, and beyond this size the structures do not correspond to any of the structural forms commonly found in clusters. However, these latter clusters are not simply disordered. High symmetry, magic number clusters are still present, the most prominent of which is the 148-atom  $D_{3d}$  hexagonal barrel. We relate these structural preferences back to the form of the interactions.

PACS numbers: 61.46.+w,36.40.Mr

## I. INTRODUCTION

The structure of a cluster is one of its primary properties and one which has been intensely studied, experimentally and theoretically [1, 2]. However, there is still much to be learnt about the fundamentals of cluster structure and the possible structures that can be formed. For atomic clusters with pair interactions, it is relatively well-understood how the form of the potential determines the observed structure. For example, the effects of the width of the potential well [3, 4] and oscillations in the potential [5–7] have been systematically studied. However, for the systems that are of most interest, the interatomic interactions are usually much more complex. In particular, metal clusters, which are of great technological relevance [8], have a strong many-body character to their bonding.

This presents a number of challenges to our understanding of cluster structure in metals. First, there is the possibility that new types of structure could emerge as a result of many-body effects. Although, the structural types observed for pair potentials are also frequently observed for metals, e.g. the competition between icosahedral, decahedral and close-packed structures is also common for metals [9], there are an increasing number of intriguing exceptions. One seemingly common feature for small metal clusters is to exhibit structures with no discernible order [10–14]. However, it might be that the disorder is a result of new structural principles that cannot be fully satisfied at the sizes considered (hence the disorder), but which could lead to novel high symmetry structures at certain magic sizes [15]. Indeed, there are general grounds to expect high symmetry structures to emerge irrespective of the potential [16]. Studies that just reoptimize known cluster structures will of course miss such new features, and so it is important that efficient global optimization algorithms are used.

Secondly, the many-body character makes it increasingly difficult to relate the observed structure back to the interactions, even when the assumed form for the many-body potential is relatively simple. There has been some interesting progress recently in this area, namely into the causes of the disordered structures [17], and the effect of the range of the attraction and repulsion on the competition between icosahedral, decahedral and close-packed clusters [18], but there is much still to be discovered. This task is particularly important because of the difficulty in producing good empirical metal potentials (it is not feasible to study the sizes in which we are interested in any other way). One needs this kind of physical insight to understand the strengths and deficiencies of a potential and how it could be improved. It would also help one to discriminate between different potentials that purport to model the same material but give rise to different structures.

Lead clusters illustrate some of these challenges. The first theoretical study on large clusters by Lim *et al.* using a glue potential seemed to indicate that the most stable clusters at relatively small sizes (from at least  $N \sim 55$ ) are face-centred cubic (fcc) [19], the preferred bulk structure [20]. This conclusion was based on a comparison of the energies of a series of Mackay icosahedra and fcc cuboctahedra. It is quite unusual to see bulk structures already being favoured at such small sizes, but this finding was rationalized on the basis of the particularly small value of  $\gamma$ , the ratio of the surface energies of the  $\{100\}$  and  $\{111\}$  faces [19]. Usually, the Mackay icosahedra have an energetic advantage at small sizes, because exclusively having  $\{111\}$  facets gives them an appreciably lower surface energy. Furthermore, these results were not inconsistent with the experiments in the literature at that time, which were mass spectroscopic studies on very small lead clusters [21, 22], and electron diffraction experiments on very large clusters, which were identified as fcc, but with possibly some vestiges of amorphous structure [23].

This basic picture though has recently been challenged

---

\*jpkd1@cam.ac.uk; <http://www-wales.ch.cam.ac.uk/~jon>

by both experimental [24] and theoretical [25] results. Electron diffraction of clusters from 3 to 7 nm indicates that the largest clusters are dominated by decahedra, but for the smaller clusters it was not possible to obtain an adequate fit to the diffraction pattern, suggesting that alternative structural models need to be considered [24].

Simulations of the melting and freezing of large lead clusters (modelled by the glue potential used by Lim *et al.* [19]) unexpectedly revealed that for a certain size range ( $600 < N < 4000$ , at least) fcc structures are not lowest in energy [25]. Instead, a new type of icosahedral structure, which is more stable than the fcc structures, spontaneously formed both on freezing and on heating at temperatures just below that for melting. Similar structures had been previously seen in some simulations of large lead clusters but it was not recognised that they could be lowest in energy [26]. They resemble anti-Mackay icosahedra [27], which have a Mackay icosahedral core but with most of the outer layer in ‘hexagonal close-packed’ (hcp) surface sites rather than the ‘fcc’ sites that would continue the packing in the Mackay icosahedra.

These results naturally raise intriguing questions about the structures of small lead clusters. What alternative structural models might be needed to understand the experimental results? Do lead clusters, as modelled by the glue potential, really favour fcc structures at small sizes? Lim *et al.* clearly showed that other standard forms were not lower in energy, so the structures would have to be somewhat unusual. Interestingly, a simple analysis using macroscopic properties as inputs suggested that lead would be a particular likely candidate for disordered clusters to be low in energy [17].

Here, we address some of these issues by performing global optimization for lead clusters with up to 160 atoms. We pay particular attention to characterizing the structures of these clusters and to understanding why the potential favours the lowest-energy structures.

## II. METHODS

To model the lead clusters we use a glue potential [28] of the form

$$E = \sum_{i < j} \phi(r_{ij}) + \sum_i U(n_i), \quad (1)$$

where  $\phi(r)$  is a short-ranged pair potential,  $U(n)$  is a many-body glue function and  $n_i$  is a “generalized coordination number” for atom  $i$ .  $n_i$  is defined as

$$n_i = \sum_j \rho(r_{ij}), \quad (2)$$

where  $\rho(r)$  is an “atomic density” function. These three functions have been fitted for lead using a variety of bulk and surface properties [19]. The use of surface energies is particularly important for the application of this potential to model clusters. As well as clusters, this potential

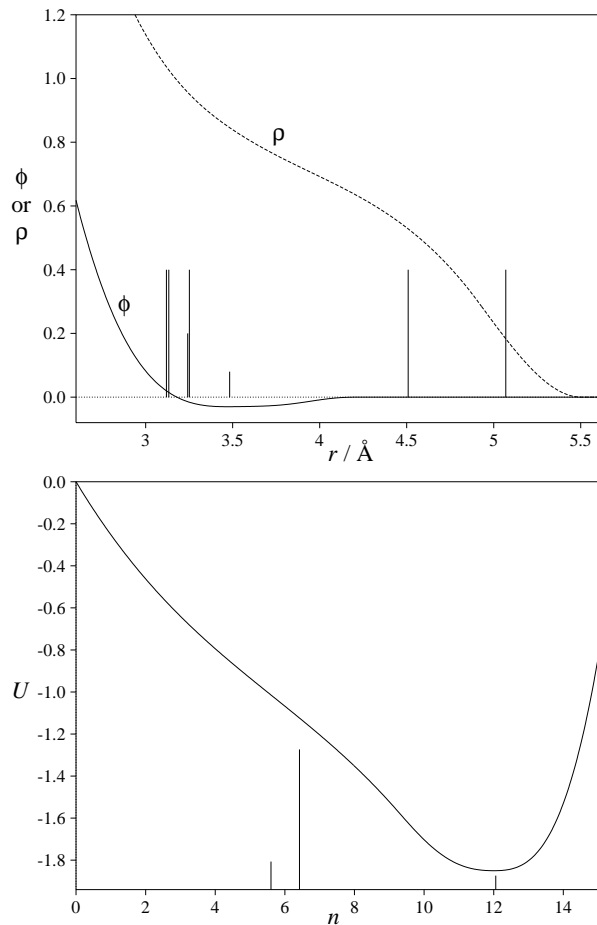


FIG. 1: The three functions that make up the lead glue potential: (a)  $\phi(r)$ ,  $\rho(r)$  and (b)  $U(n)$ . The pair distances and  $n_i$  values in the 13-atom decahedron are also plotted as impulses, with the heights proportional to the number that take that value.

has been also used to model the surface reconstructions and pre-melting of low-index lead surfaces [29, 30], and lead nanowires [31, 32].

The choice of this empirical potential is motivated by the need for computational efficiency in order that global optimization is feasible for the sizes we consider here, and by our intention to compare with previous results. The use of *ab initio* electronic structure methods for lead is prohibitively expensive, especially as relativistic effects would need to be included to obtain reasonable results [20]. For example, sophisticated density functional calculations are unable to reproduce the experimental surface energies and anisotropies [33, 34].

The functions  $U(n)$ ,  $\phi(r)$  and  $\rho(r)$  are displayed in Figure 1. The pair potential has a very shallow well and so most of the binding energy comes from the glue term. The glue term has been chosen to have its minimum at  $n=12$ , consistent with the designation of  $n$  as an effective coordination number. The form of  $\rho(r)$  is particularly significant. As  $\rho(r)$  decreases relatively slowly with increasing  $r$  beyond the minimum in the pair potential,

next-nearest neighbours make a significant contribution to  $n$ . Therefore, the difference in surface energies between the  $\{111\}$  and  $\{100\}$  faces is small because, although an atom on a  $\{111\}$  face has fewer nearest neighbours, it has more next-nearest neighbours [19]. However,  $\rho(r)$  then decreases relatively rapidly to zero at the cutoff at  $r = 5.503\text{\AA}$ , which typically occurs between the second and third neighbour shells.

For a pair potential the pair distances are the most important quantities. For example, the lowest-energy structure of a cluster involves a balance between maximization of the number of nearest neighbours, whilst minimizing the strain energy that results from nearest-neighbour pair distances deviating from the equilibrium pair value,  $r_{\text{eq}}$  [3]. However, for a glue potential, such as the current one, where the main contribution to the energy is from the glue function, the most important quantities are the  $n_i$ . Indeed, one of the key factors in generating a low-energy structure is to have the  $n_i$  values as close as possible to  $n_{\text{eq}}$ , the value of  $n$  at the minimum of  $U$ . This can potentially lead to different ordering principles than for pair potentials. Only structures that have their nearest-neighbour pair distances close to  $r_{\text{eq}}$  are generally competitive for pair potentials. However, this constraint is relaxed for glue potentials, and particularly when, as in the current case,  $\rho(r)$  initially falls off weakly with  $r$ .

For the atoms on the surface of a cluster  $n_i < n_{\text{eq}}$ . Therefore, there will be a driving force for contraction of the surface to make the pair distances for the surface atoms smaller and hence their  $n_i$  larger. At equilibrium the surface contraction will be balanced by the increase in energy due to the resulting compression of the cluster core.

These considerations represent a particular problem for some of the usual forms for atomic clusters, such as the Mackay icosahedra and to a lesser extent decahedra. The inherent strain in these clusters results in pair distances between surface atoms that are longer than  $r_{\text{eq}}$ , and so the compression needed to increase  $n_i$  for the surface atoms is particularly large. Therefore, these traditional structural forms are expected to become increasingly disfavoured by potentials for which the pair separation depends strongly on coordination number [17]. Instead, novel forms that are able to obtain large  $n_i$  values for the surface atoms, whilst not having too large an energetic penalty for compression of the cluster interior, could potentially be lowest in energy.

The global optimization of the lead clusters was performed using the basin-hopping [35, 36] (or Monte Carlo minimization [37]) approach. This method has proved particularly successful in locating putative global minima for a wide variety of cluster systems [38]. The optimization task becomes rapidly more difficult with increasing  $N$  (e.g. the number of minima on the potential energy surface is thought to scale exponentially with  $N$  [39–41]) and so, of course, the possibility that we have not been able to obtain the true global minimum increases. However, the structural principles and trends are clear from

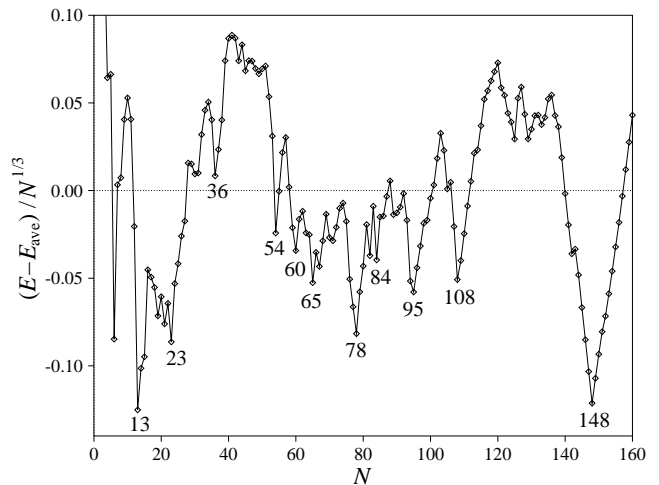


FIG. 2: Energies of the putative global minima relative to  $E_{\text{ave}}$ , a four-parameter fit to these energies.  $E_{\text{ave}} = -2.0251N + 1.6608N^{2/3} + 1.3662N^{1/3} - 0.8634$

our results.

### III. GLOBAL MINIMA FOR $N \leq 160$

The energies and point groups for the putative global minima are given in Table I. Point files will be made available online at the Cambridge Cluster Database [38]. The energies of the global minima are represented in Figure 2 in such a way that makes particularly stable clusters stand out. All clusters in the range  $9 \leq N \leq 40$  are depicted in Figure 3 and a selection of particularly stable larger clusters in Figure 4.

First, we will look at the global minima for  $N \leq 40$  in detail, before surveying more briefly the results for larger clusters. For  $N \leq 8$  the clusters exhibit the same structures as typically seen for pair potentials. However,  $\text{Pb}_9$  has a somewhat unusual form that can be described as two face-sharing octahedra, and so, as with  $\text{Pb}_{10}$ , is the beginning of an hcp cluster. Then for  $N=11$  and 12 more open structures with three-fold axes of symmetry are preferred.

Most of the global minima for  $13 \leq N \leq 33$  are decahedral in origin. However, the growth sequence is not straightforward. The decahedra are generally asymmetric with the quasi-fivefold axis not passing through the centre of mass. So, although the growth sequence begins by adding atoms around the equator of the 13-atom Ino decahedron [42], before this shell is completed, asymmetric decahedra with a longer quasi-fivefold axis become lower in energy, starting at  $N=21$ . Furthermore, sometimes part of the structure is distorted away from the ideal decahedral positions, e.g. at  $N=18, 19, 26$  and 32. There are also structures with two interpenetrating ( $\text{Pb}_{20}$ ) and face-sharing ( $\text{Pb}_{24}$ ) 13-atom decahedra, the latter with two additional shared capping atoms. It is noticeable that the decahedral global minima generally

TABLE I: Energies and point groups (PG) of the putative global minima.

$N$	PG	Energy/eV	$N$	PG	Energy/eV	$N$	PG	Energy/eV	$N$	PG	Energy/eV
3	$D_{3h}$	-1.380851	43	$C_s$	-62.518056	83	$C_1$	-131.453946	123	$C_2$	-201.844885
4	$T_d$	-2.558548	44	$C_s$	-64.158589	84	$D_2$	-133.335862	124	$C_2$	-203.652142
5	$D_{3h}$	-3.711742	45	$C_s$	-65.887013	85	$C_1$	-134.977705	125	$C_1$	-205.483134
6	$O_h$	-5.214277	46	$C_1$	-67.545017	86	$C_2$	-136.725287	126	$C_1$	-207.149663
7	$D_{5h}$	-6.342793	47	$C_1$	-69.227454	87	$C_1$	-138.426910	127	$C_1$	-208.901679
8	$C_{2v}$	-7.665775	48	$C_1$	-70.926964	88	$C_1$	-140.139735	128	$C_1$	-210.764087
9	$D_{3h}$	-8.962242	49	$C_2$	-72.624639	89	$C_{2v}$	-141.978803	129	$C_1$	-212.620619
10	$C_{2v}$	-10.328111	50	$C_1$	-74.303601	90	$C_s$	-143.728686	130	$C_1$	-214.378335
11	$C_{3v}$	-11.771970	51	$C_1$	-75.989247	91	$C_{2v}$	-145.469445	131	$C_1$	-216.125616
12	$D_{3h}$	-13.351511	52	$C_1$	-77.748769	92	$C_1$	-147.190877	132	$C_1$	-217.911017
13	$D_{5h}$	-15.060197	53	$C_1$	-79.529727	93	$C_1$	-149.017327	133	$C_1$	-219.726303
14	$C_{2v}$	-16.488673	54	$S_{10}$	-81.438379	94	$C_{2v}$	-150.933479	134	$C_1$	-221.493988
15	$C_{2v}$	-17.971698	55	$C_1$	-83.050627	95	$C_{2v}$	-152.722173	135	$C_1$	-223.228659
16	$C_{2v}$	-19.359118	56	$C_1$	-84.670414	96	$C_s$	-154.419817	136	$C_1$	-225.006412
17	$C_{3v}$	-20.892141	57	$C_1$	-86.343451	97	$C_1$	-156.124859	137	$C_1$	-226.856548
18	$C_1$	-22.441282	58	$C_1$	-88.160853	98	$C_1$	-157.827739	138	$C_2$	-228.680493
19	$C_{2v}$	-24.029140	59	$C_1$	-89.961499	99	$C_1$	-159.582628	139	$C_1$	-230.562421
20	$C_{2v}$	-25.554526	60	$C_1$	-91.725507	100	$C_1$	-161.288978	140	$C_1$	-232.461447
21	$C_{2v}$	-27.160557	61	$C_1$	-93.369916	101	$C_1$	-163.018692	141	$C_1$	-234.347193
22	$C_1$	-28.700367	62	$C_1$	-95.068322	102	$C_1$	-164.713475	142	$C_1$	-236.226662
23	$C_{2v}$	-30.342369	63	$C_1$	-96.835577	103	$C_1$	-166.412388	143	$C_1$	-238.007461
24	$D_{2h}$	-31.834411	64	$C_2$	-98.559680	104	$C_1$	-168.225729	144	$C_2$	-239.879381
25	$C_{2v}$	-33.394629	65	$C_2$	-100.391525	105	$C_1$	-170.097176	145	$C_s$	-241.772812
26	$C_s$	-34.947504	66	$S_4$	-102.045664	106	$C_1$	-171.848423	146	$C_2$	-243.665845
27	$C_{2v}$	-36.526823	67	$C_1$	-103.803493	107	$C_s$	-173.738048	147	$C_s$	-245.558654
28	$C_1$	-38.036722	68	$C_1$	-105.470725	108	$C_{2v}$	-175.653403	148	$D_{3d}$	-247.451751
29	$C_s$	-39.653184	69	$C_1$	-107.136603	109	$C_{2v}$	-177.373836	149	$C_1$	-249.175286
30	$C_s$	-41.291166	70	$C_1$	-108.921031	110	$C_s$	-179.073251	150	$C_s$	-250.900806
31	$C_{2v}$	-42.914946	71	$C_2$	-110.659704	111	$C_{2v}$	-180.771206	151	$C_1$	-252.632151
32	$C_{2v}$	-44.475555	72	$C_1$	-112.360587	112	$C_s$	-182.477331	152	$C_2$	-254.384256
33	$C_1$	-46.064990	73	$C_1$	-114.048803	113	$C_s$	-184.174089	153	$C_1$	-256.115829
34	$C_1$	-47.687973	74	$C_1$	-115.771829	114	$C_2$	-185.939956	154	$C_2$	-257.846941
35	$C_s$	-49.363201	75	$C_1$	-117.552036	115	$C_1$	-187.649103	155	$C_1$	-259.573483
36	$D_{3d}$	-51.115236	76	$C_2$	-119.429639	116	$C_1$	-189.351898	156	$C_2$	-261.299215
37	$C_{3v}$	-52.716480	77	$C_1$	-121.236712	117	$C_1$	-191.105099	157	$C_1$	-263.019401
38	$D_{3d}$	-54.314542	78	$C_2$	-123.043586	118	$C_1$	-192.855140	158	$C_2$	-264.738883
39	$C_1$	-55.857448	79	$C_2$	-124.684422	119	$C_1$	-194.607282	159	$C_1$	-266.456122
40	$C_2$	-57.474215	80	$C_1$	-126.364903	120	$C_1$	-196.361528	160	$C_1$	-268.174733
41	$C_s$	-59.130894	81	$C_1$	-128.007123	121	$C_1$	-198.211397			
42	$C_s$	-60.803249	82	$D_3$	-129.829950	122	$C_1$	-200.012938			

have a significant proportion of surface atoms in  $\{100\}$  type environments. This feature reflects the small energy difference between fcc  $\{111\}$  and  $\{100\}$  faces noted earlier. For materials that more strongly favour  $\{111\}$  faces, the most stable decahedral form is usually a Marks decahedron [43], because this structure maximizes the proportion of  $\{111\}$  faces, whilst retaining a relatively spherical shape. However, for lead the most stable decahedral

clusters occur at  $N=13$  and  $23$  (Figure 2).

The other set of ordered global minima found for  $N \leq 40$  are the hcp clusters at  $N=35-38$ . Again, these structures are somewhat unexpected, particularly as the fcc truncated octahedron is possible at  $N=38$ , but this is further evidence of a preference for structures with a significant proportion of  $\{100\}$ -like faces.

Of the other global minima for  $N \leq 40$ ,  $Pb_{17}$  is related

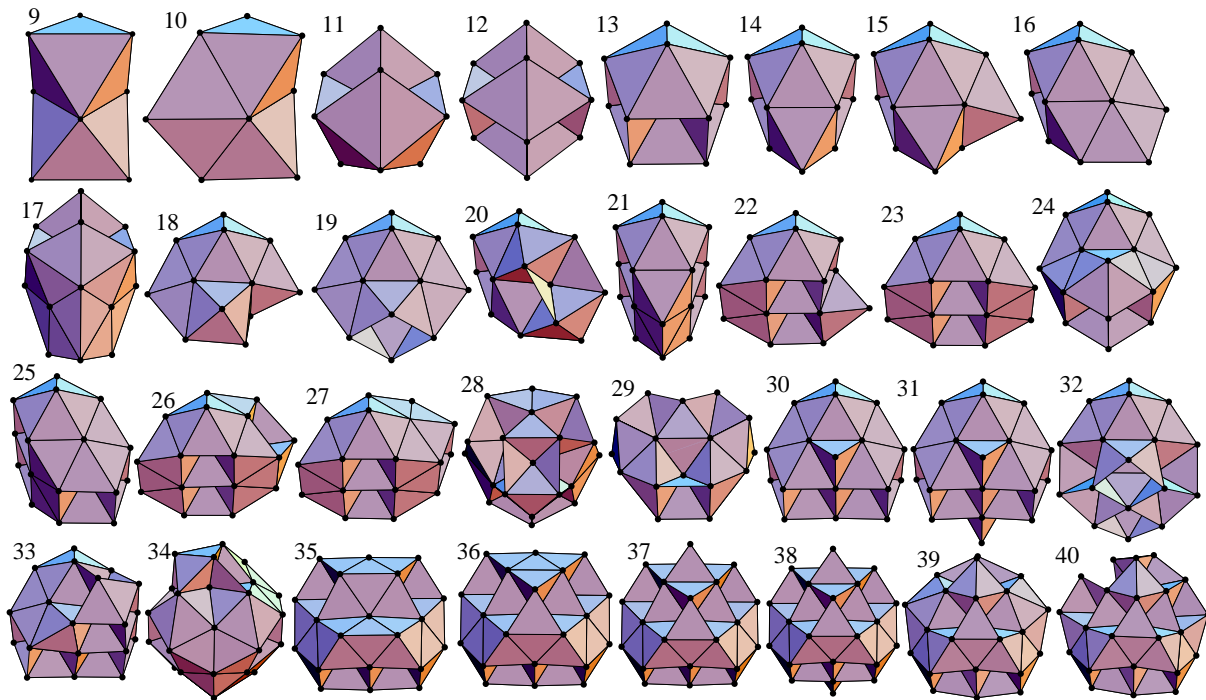


FIG. 3: The global minima for  $N \leq 40$ . Each cluster is labelled by the value of  $N$ .

to the 11-atom global minimum, but it is hard to discern any overall order for those at  $N=28, 29$  and  $34$ .  $Pb_{39}$  and  $Pb_{40}$  are somewhat related to the preceding hcp structures, as is clear from the viewpoint chosen for Figure 3, but again there is little order apparent on the other side of the cluster.

Beyond  $N=38$  none of the global minima that we have located can be assigned to any of the usual structural forms. However, it would be too simplistic just to characterize the clusters as disordered. From Table I we can see that high symmetry structures are still present. Furthermore, if the clusters were just disordered one would expect cluster properties to evolve fairly smoothly with size. However, it is clear from Figure 2 that there are “magic number” clusters that are particularly low in energy. Unsurprisingly, these magic numbers often correspond to the high symmetry clusters.

Although most of the clusters in this size range have no discernible *overall order*, there are common local surface motifs that are repeatedly visible. However, only at a relatively few sizes can these local preferences be assembled into a structure that has clear overall order.

As for the smaller clusters the surface structures of the global minima reflect the particularly low value of  $\gamma$ . However, this does not lead to structures with large  $\{100\}$  faces, but rather to many surface atoms with  $\{100\}$ -like environments. The surfaces are typically covered with a patchwork of squares and triangles. So on the flat regions of the surface it is common to see atoms surrounded by three triangles and two squares (there are two ways this can be achieved), rather than the six triangles or four

squares, that are typical of  $\{111\}$  and  $\{100\}$  surfaces, respectively.

$Pb_{54}$  is somewhat related to the Mackay icosahedron. It has an uncentred 13-atom icosahedron at its centre and a clear five-fold axis of symmetry. Along this axis it looks similar to the the  $D_{5h}$  structure that was found by Wolf and Landman as a low-energy isomer of the 55-atom Lennard-Jones clusters [44], and which is related to the icosahedron by a single rearrangement in which the structure is twisted around a five-fold axis. However, there is a canted arrangement of squares and triangles around the equator of the cluster.

The axial configuration of  $Pb_{54}$  seems to be quite a common motif, and similar patterns can be seen in one of the chosen views for  $N=60, 78, 95$  and  $148$ , the last based on a six-fold rather than a five-fold symmetric version of the pattern, thus making the top surface flat, rather than pyramidal. As the size of these clusters increases the pattern is, of course, extended outwards. The resulting motif is clearest for the highly symmetric, 148-atom global minimum.

$Pb_{148}$  is the most prominent magic number in this size range (Figure 2). In shape, the cluster is a hexagonal barrel. Although the outer surface has a clear sixfold symmetry, this is in fact broken by the octahedron at the centre of the cluster.

As flagged in the introduction, an important aim of this paper is not only to characterize the global minima for this lead potential, but to understand how the observed structures relate back to the form of the potential. We start by examining the decahedral 13-atom

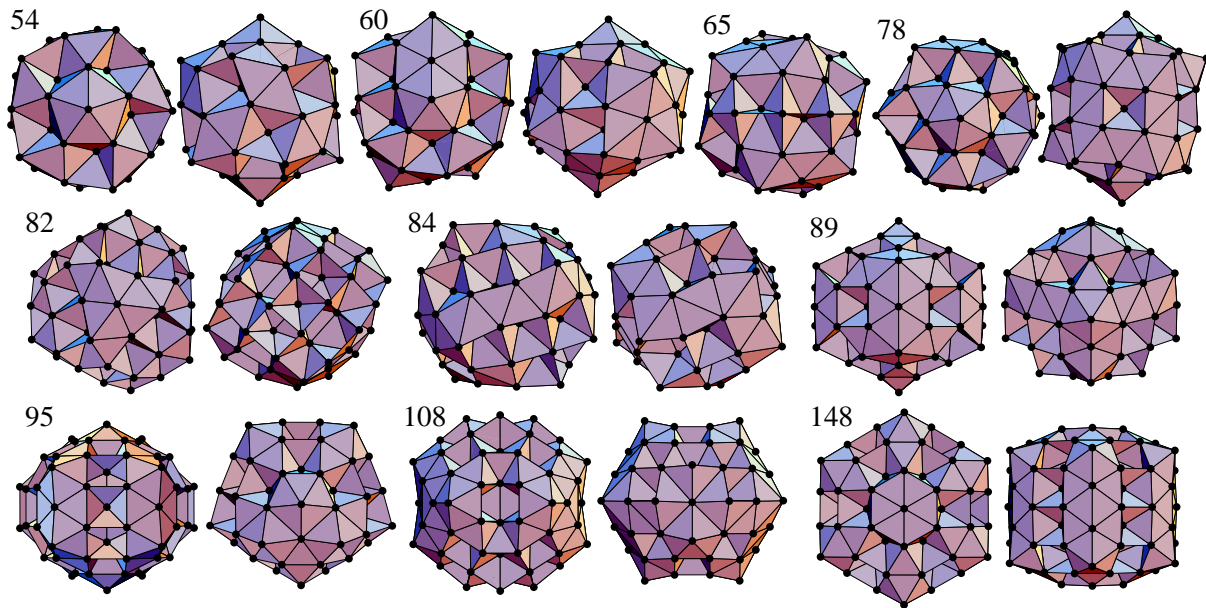


FIG. 4: A selection of particularly stable global minima for  $N > 40$ . Each cluster is labelled by the value of  $N$ . For most of the clusters two perpendicular views of the structure are given.

TABLE II: The contributions to the energy for a series of 55-atom structures, namely the global minimum ( $C_1$ ), the fcc cuboctahedron ( $O_h$ ), the Ino decahedron ( $D_{5h}$ ) and the Mackay icosahedron ( $I_h$ ). The structures are denoted by their point group (PG).  $\langle E_i^{\text{bulk}} \rangle$  and  $\langle E_i^{\text{surf}} \rangle$  are the average atomic energies for atoms in the interior of the cluster and on the surface, respectively. All the energies are measured in eV.

PG	Energy	$E_{\text{pair}}$	$n_{\text{nn}}$	$E_{\text{strain}}$	$E_{\text{glue}}$	$\langle n_i \rangle$	$\langle E_i^{\text{bulk}} \rangle$	$\langle E_i^{\text{surf}} \rangle$
$C_1$	-83.051	-1.796	216	4.684	-81.254	9.072	-1.885	-1.405
$O_h$	-82.559	-4.338	216	2.142	-78.220	8.783	-1.956	-1.360
$D_{5h}$	-82.438	-4.248	219	2.322	-78.190	8.800	-1.933	-1.365
$I_h$	-81.295	-5.944	234	1.076	-75.351	8.500	-1.946	-1.333

global minimum, for which the  $r_{ij}$  and  $n_i$  values have been included in Figure 1. It is noticeable that there is a significant dispersion of nearest-neighbour distances. In fact the longest distance is 11.7% longer than the shortest, which compares to a 2.3% difference for the same structure when optimized for the Lennard-Jones potential. As expected from the discussion in Section II, the structure distorts to move the  $n_i$  values as close to  $n_{\text{eq}}$  as possible, rather than keeping the nearest-neighbour distances near to the minimum of the pair potential. This is achieved by an expansion along the fivefold axis and a contraction of the equator of the cluster. This reduces the  $n_i$  values for the two vertex atoms on the fivefold axis, but increases the  $n_i$  values for the other ten surface atoms, while maintaining the  $n_i$  value for the central atom close to  $n_{\text{eq}}$ . A similar anisotropy of the pair distances has previously been noted by Lim *et al.* in their analysis of the lead cuboctahedra [19]; there is a greater contraction

for the  $\{100\}$  faces of the cuboctahedra than the  $\{111\}$  faces because of the enhanced contribution to  $n_i$  from next neighbours across the diagonals of the squares on the  $\{100\}$  faces.

To understand why novel structural forms are observed for this lead potential, we take  $\text{Pb}_{55}$  as an example and compare the contributions to the energy from a series of competing structures (Table II and Figure 5). The global minimum is based on the 54-atom structure illustrated in Figure 4 but with an additional surface atom. Also possible at this size are a fcc cuboctahedron, an Ino decahedron and a Mackay icosahedron.

In Table II we have decomposed the pair energy into two components:

$$E_{\text{pair}} = -n_{\text{nn}}\epsilon + E_{\text{strain}}, \quad (3)$$

where  $n_{\text{nn}}$  is the number of nearest neighbours,  $\epsilon$  is the depth of the pair potential, and  $E_{\text{strain}}$  is the energetic penalty for distances that deviate from  $r_{\text{eq}}$ , the distance corresponding to the minimum of the pair potential. More formally,

$$E_{\text{strain}} = \sum_{i < j, r_{ij} < r_0} \epsilon - \phi(r_{ij}), \quad (4)$$

where  $r_0$  is a distance criterion that distinguishes nearest from next-nearest neighbours. For all the structures we consider, there is a clear separation between these coordination shells.

As expected the pair energy only contributes a small fraction of the total energy. It is also noticeable that  $E_{\text{strain}}$  is of similar magnitude to  $E_{\text{pair}}$ . This is in marked contrast to what occurs for pair potentials, where minimization of the strain energy is a key element of a struc-

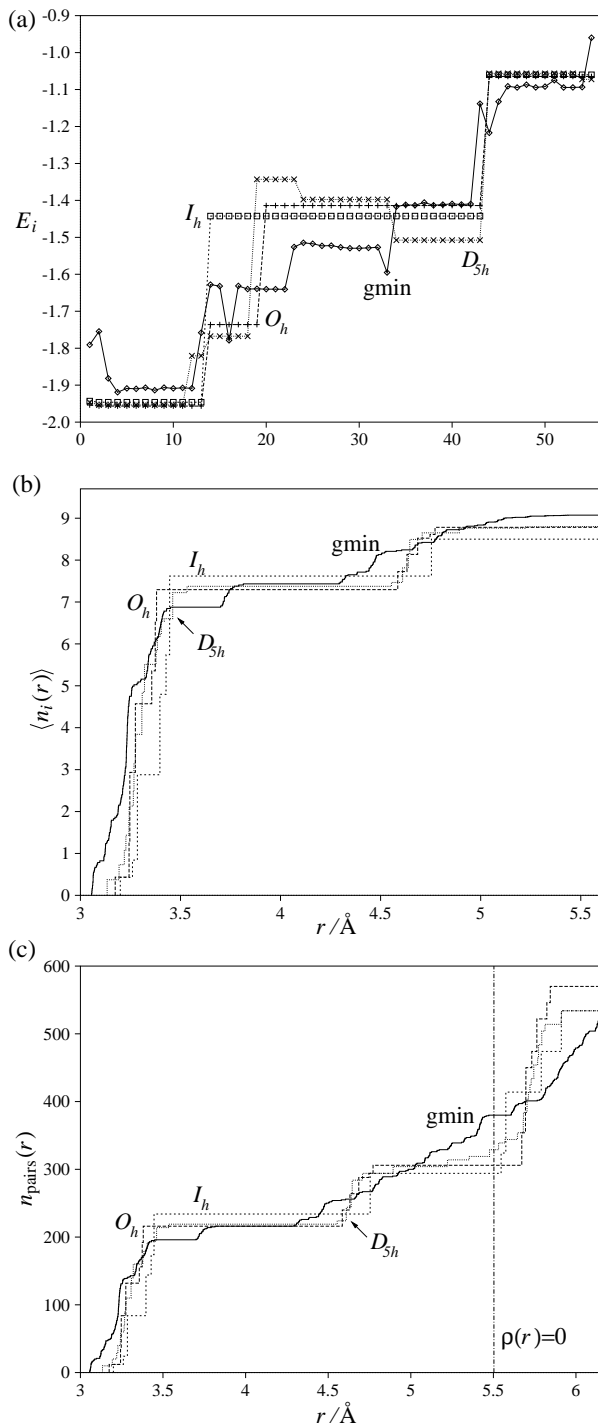


FIG. 5: A comparison of the properties of the 55-atom global minimum (gmin) to the fcc cuboctahedron ( $O_h$ ), the Ino decahedron ( $D_{5h}$ ) and the Mackay icosahedron ( $I_h$ ), the same four clusters as in Table II. (a) The atomic energies,  $E_i$ , for each atom in the cluster. The atoms have been ranked by their distance from the centre of mass, with atom 1 being the closest to the centre. (b)  $\langle n_i(r_{ij} < r) \rangle$ . (c)  $n_{\text{pairs}}(r)$ .

ture's stability.  $E_{\text{strain}}$  for the global minimum is particularly large.

Although the pair energy is small in magnitude, it is structure sensitive and so it can still determine the relative stabilities of structures when the energies from the glue term,  $E_{\text{glue}}$ , are similar. For example, the major component of the difference in energy between the 55-atom cuboctahedron and decahedron is the greater pair energy of the cuboctahedron.

It is clear from Table II that the global minimum's stability is a result of its significantly lower glue energy, which is a result of the atoms being able to achieve  $n_i$  values that are closer to the ideal value,  $n_{\text{eq}}$ . However, this lower glue energy is partially offset by the higher pair energy resulting from the distortion of the pair distances that is necessary to achieve an increase in  $n_i$ .

If we look at the atomic contributions to the energy (Table II and Figure 5(a)) it is clear that the lower energy results from a lower average energy for the surface atoms (particularly atoms 13–33 in Figure 5(a)), which outweighs the somewhat less favourable energies for the atoms in the interior of the cluster.

It is also interesting to understand what structural features of the global minimum lead to the larger value of  $\langle n_i \rangle$ . We analyse this in Figure 5(b) and (c), first by looking at the cumulative contribution to  $\langle n_i \rangle$  from pairs with distances less than  $r$ :

$$\langle n_i(r_{ij} < r) \rangle = \frac{1}{N} \sum_{i \neq j, r_{ij} < r} \rho(r_{ij}). \quad (5)$$

It is particularly interesting to note that  $\langle n_i^<(r) \rangle$  for the global minimum only becomes largest beyond  $4.926\text{\AA}$ . Therefore, although the contribution to  $\langle n_i \rangle$  from distances beyond this distance is small in magnitude, it is key in stabilizing the global minimum relative to the more conventional forms.

We can analyse this further by considering  $n_{\text{pairs}}(r)$ , the number of pairs of atoms that are separated by less than  $r$ . It can be seen from Figure 5(c) that the number of pair distances within the radius of the cutoff distance for  $\rho$  is significantly larger for the global minimum than for the competing structures, which in turn correlates with the larger value of  $\langle n_i \rangle$ . However, this is only true because the cutoff is located between the second and third coordination shell. The cuboctahedron, decahedron and icosahedron all have a relatively narrow distribution of nearest-neighbour distances, which leads to a clear distinction between the second and third coordination shell. By contrast, the global minimum has a much more disperse nearest-neighbour shell and hence there is no clear distinction between a second and third neighbour shell. Instead, there is a steady increase in  $n_{\text{pairs}}(r)$  beyond the start of the second neighbour shell.

Although the above analysis has been presented for a single cluster, repeating this procedure for other sizes has confirmed the generality of the conclusions.

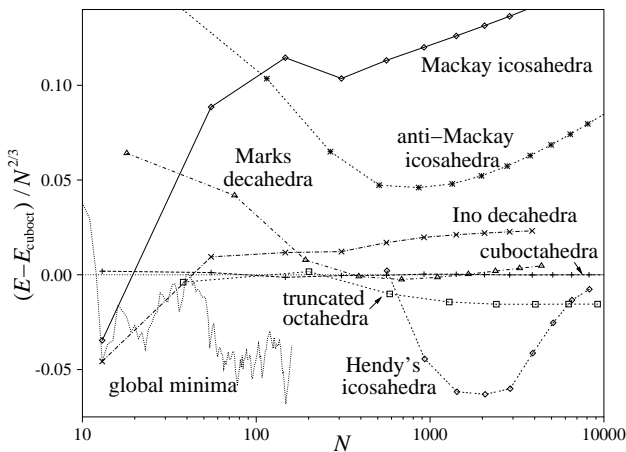


FIG. 6: A comparison of the energies of the global minima and the new icosahedra discovered by Hendy [25, 45], to series of high-symmetry structures, which include Mackay and anti-Mackay icosahedra, cuboctahedra, truncated octahedra (with regular hexagonal  $\{111\}$  faces), Ino decahedra and Marks decahedra. The energies are measured with respect to  $E_{\text{cuboct}} = -2.0284N + 1.7929N^{2/3} + 0.9714N^{1/3} - 0.6342$ .

#### IV. CONCLUSIONS

We have shown by locating the global minima for small lead clusters interacting with a many-body potential of the glue form that, contrary to the original conclusion of Lim *et al.*, these clusters do not adopt fcc geometries for  $N \leq 160$ . Instead, they form a series of novel structures that are a consequence of the many-body character of the potential. These results naturally lead one to wonder at what size bulk-like fcc structures will develop. To help us answer this question we have plotted in Figure 6 the energies of the global minima, alongside those for a number of sequences of high-symmetry structures and the novel icosahedral forms that Hendy obtained by simulations of freezing [25] and by construction [45].

The figure confirms that the icosahedra and decahedra are always higher in energy than the best fcc structures (except at the smaller sizes considered in the last section) and that the fcc truncated octahedra become slightly lower in energy than the cuboctahedra [19, 25]. More interestingly, we can clearly see that both the global minima we have found and the new icosahedra produced by Hendy [25, 45] are significantly lower in energy than the best fcc clusters. Thus, extrapolations between these two size ranges [46] suggest that fcc clusters might well not be the lowest in energy for intermediate sizes, and hence that fcc clusters are not lowest in energy until at least  $N \sim 15000$  [45]. This is a surprising result, for although it is not uncommon to find small ( $N < 100$ ) metal clusters that do not exhibit any of the usual cluster structures, it is unprecedented for this behaviour to

persist up to such large sizes.

The results are also relevant to the ongoing issue of disordered metal clusters. Like recent theoretical results for gold [10–12], cadmium, zinc [14] and vanadium [13] many of our global minima do not fit with the fcc, hcp, decahedral and icosahedral structures that are often found for close-packed materials. However, to call these lead clusters disordered would be too strong because, although most of the clusters for  $N > 40$  have no overall structural order, there are common local structural preferences which at a few sizes result in highly symmetric ordered structures that are particularly stable.

For pair potentials, clusters tend to retain a lattice structure away from the magic numbers, because it is unfavourable for the pair distances to deviate significantly from the equilibrium value. For example, most small Lennard-Jones clusters can be considered to be based upon Mackay icosahedra, either with an incomplete outer layer or covered by an ordered overlayer [47]. By contrast, for metal clusters the many-body character of the bonding can make it favourable to break the lattice structure away from the magic numbers so that the atoms can (in the language of the current potential) increase their effective coordination numbers ( $n_i$ 's). A structure with no overall order results. Therefore, if one only examines a few cluster sizes the presence of particularly stable ordered structures may be missed.

From our analysis of the energetics of the competing structural forms we have seen that the shape of  $\rho(r)$ , in particular the shoulder and the position of the cutoff, is key to the stability of the novel structures that we find to be lowest in energy. This dependence on the cutoff is somewhat worrying both because it is a rather long-range feature of the potential and because its position is not physically motivated, but chosen more for computational convenience. These results illustrate how sensitively cluster structure depends on the potential; the correct determination of the relative energies of competing clusters is a stringent test of any potential [48].

Our results also help us to understand the structures exhibited by lead nanowires [31] modelled using the same potential. Gülseren *et al.* were surprised at the apparent contradiction between the non-fcc character of their nanowires and the cluster results of Lim *et al.* [19], and so suggested a number of reasons for the differing structural tendencies. However, our results show that the non-fcc character is common to both systems.

#### Acknowledgments

J.P.K.D is grateful to the Royal Society for the award of a University Research Fellowship. S.C.H. would like to acknowledge the support of the ISAT linkages fund administered by the Royal Society of New Zealand.



- 
- [1] R. L. Johnston, *Atomic and Molecular Clusters* (Taylor & Francis, London, 2002).
- [2] J. A. Alonso, *Chem. Rev.* **100**, 637 (2000).
- [3] J. P. K. Doye, D. J. Wales, and R. S. Berry, *J. Chem. Phys.* **103**, 4234 (1995).
- [4] J. P. K. Doye and D. J. Wales, *J. Chem. Soc., Faraday Trans.* **93**, 4233 (1997).
- [5] J. P. K. Doye, D. J. Wales, and S. I. Simdyankin, *Faraday Discuss.* **118**, 159 (2001).
- [6] J. P. K. Doye and D. J. Wales, *Phys. Rev. Lett.* **86**, 5719 (2001).
- [7] J. P. K. Doye, D. J. Wales, F. H. Zetterling, and M. Dzugutov, (cond-mat/0205374).
- [8] A. M. Argo, J. F. Odzak, F. Lai, and B. C. Gates, *Nature* **415**, 623 (2002).
- [9] C. L. Cleveland and U. Landman, *J. Chem. Phys.* **94**, 7376 (1991).
- [10] I. L. Garzón, K. Michaelian, and M. R. Beltrán, *Phys. Rev. Lett.* **81**, 1600 (1998).
- [11] K. Michaelian, N. Rendón, and I. L. Garzón, *Phys. Rev. B* **60**, 2000 (1999).
- [12] I. L. Garzón, C. Rovira, K. Michaelian, M. R. Beltrán, P. Ordejón, J. Junquera, D. Sanchez-Portal, E. Artacho, and J. Soler, *Phys. Rev. Lett.* **85**, 5250 (2000).
- [13] A. Taneda, T. Shimuzu, and Y. Kawazoe, *J. Phys.-Condens. Mat.* **13**, L305 (2001).
- [14] K. Michaelian, M. R. Beltrán, and I. L. Garzón, *Phys. Rev. B* **65**, 041403(R) (2002).
- [15] J. M. Soler, I. L. Garzón, and J. D. Joannopoulos, *Solid State Commun.* **117**, 621 (2001).
- [16] D. J. Wales, *Chem. Phys. Lett.* **285**, 330 (1998).
- [17] J. M. Soler, M. R. Beltrán, K. Michaelian, I. L. Garzón, P. Ordejón, D. Sánchez-Portal, and E. Artacho, *Phys. Rev. B* **61**, 5771 (2000).
- [18] F. Baletto, R. Ferrando, A. Fortunelli, F. Montalenti, and C. Mottet, *J. Chem. Phys.* **116**, 3856 (2002).
- [19] H. S. Lim, C. K. Ong, and F. Ercolessi, *Surf. Sci.* **269/270**, 1109 (1992).
- [20] D. A. Young, *Phase diagrams of the elements* (University of California Press, Berkeley, 1991).
- [21] K. LaiHing, R. G. Wheeler, W. L. Wilson, and M. A. Duncan, *J. Chem. Phys.* **87**, 3401 (1987).
- [22] J. Mühlbach, P. Pfau, K. Sattler, and E. Recknagel, *Phys. Lett. A* **87**, 415 (1982).
- [23] A. Yokozeki, *J. Chem. Phys.* **68**, 3766 (1978).
- [24] M. Hyslop, A. Wurl, S. A. Brown, B. D. Hall, and R. Monot, *Eur. Phys. J. D* **16**, 233 (2001).
- [25] S. C. Hendy and B. D. Hall, *Phys. Rev. B* **64**, 085425 (2001).
- [26] H. S. Lim, C. K. Ong, and F. Ercolessi, *Comput. Mater. Sci* **2**, 495 (1994).
- [27] J. P. K. Doye and D. J. Wales, *Z. Phys. D* **40**, 466 (1997).
- [28] F. Ercolessi, M. Parrinello, and E. Tosatti, *Philos. Mag. A* **58**, 213 (1988).
- [29] C. P. Toh, C. K. Ong, and F. Ercolessi, *Phys. Rev. B* **50**, 17507 (1994).
- [30] A. Landa, P. Wynblatt, H. Häkkinen, R. N. Barnett, and U. Landman, *Phys. Rev. B* **51**, 10972 (1995).
- [31] O. Gülseren, F. Ercolessi, and E. Tosatti, *Phys. Rev. Lett.* **80**, 3775 (1998).
- [32] O. Gülseren, F. Ercolessi, and E. Tosatti, *Phys. Rev. B* **51**, 7377 (1995).
- [33] L. Vitos, A. V. Ruban, H. L. Skriver, and J. Kollár, *Surf. Sci.* **411**, 186 (1998).
- [34] P. J. Feibelman, *Phys. Rev. B* **62**, 17020 (2000); **65**, 129902(E) (2002).
- [35] D. J. Wales and J. P. K. Doye, *J. Phys. Chem. A* **101**, 5111 (1997).
- [36] D. J. Wales and H. A. Scheraga, *Science* **285**, 1368 (1999).
- [37] Z. Li and H. A. Scheraga, *Proc. Natl. Acad. Sci. USA* **84**, 6611 (1987).
- [38] D. J. Wales, J. P. K. Doye, A. Dullweber, M. P. Hodges, F. Y. Naumkin, F. Calvo, J. Hernández-Rojas and T. F. Middleton, The Cambridge Cluster Database, URL <http://www-wales.ch.cam.ac.uk/CCD.html>.
- [39] C. J. Tsai and K. D. Jordan, *J. Phys. Chem.* **97**, 11227 (1993).
- [40] F. H. Stillinger, *Phys. Rev. E* **59**, 48 (1999).
- [41] J. P. K. Doye and D. J. Wales, *J. Chem. Phys.* **116**, 3777 (2002).
- [42] S. Ino, *J. Phys. Soc. Jpn.* **27**, 941 (1969).
- [43] L. D. Marks, *Philos. Mag. A* **49**, 81 (1984).
- [44] M. D. Wolf and U. Landman, *J. Phys. Chem. A* **102**, 6129 (1998).
- [45] S. C. Hendy and J. P. K. Doye, *Phys. Rev. B* (to be submitted).
- [46] Although only one series of structures with the novel icosahedral form has been included in Fig. 6, many are possible, which are characterized by the number of facets that are of a certain type [45]. If the energies of all these series were calculated, the size range over which these novel icosahedra are most stable would be significantly wider than suggested by Fig. 6.
- [47] J. A. Northby, *J. Chem. Phys.* **87**, 6166 (1987).
- [48] J. P. K. Doye and D. J. Wales, *J. Chem. Phys.* **116**, 8307 (2002).